

Defect behavior during growth of heavily phosphorus doped Czochralski silicon crystals (II): Theoretical study

Cite as: J. Appl. Phys. 136, 055705 (2024); doi: 10.1063/5.0200130

Submitted: 25 January 2024 · Accepted: 27 May 2024 ·

Published Online: 1 August 2024



View Online



Export Citation



CrossMark

Koji Sueoka,^{1,a)} Yasuhito Narushima,² Kazuhisa Torigoe,³ Naoya Nonaka,³ Koutaro Koga,³ Toshiaki Ono,³ Hiroshi Horie,³ and Masataka Hourai³

AFFILIATIONS

¹ Department of Communication Engineering, Okayama Prefectural University, Soja-Shi, Okayama 719-1197, Japan

² Product and Technology Division, SUMCO TECHXIV Corporation, Omura-Shi, Nagasaki 856-8555, Japan

³ Production and Technology Division, SUMCO Corporation, Imari-Shi, Saga 849-4256, Japan

Note: This paper is part of the special topic, Defects in Semiconductors 2024.

a) Author to whom correspondence should be addressed: sueoka@c.oka-pu.ac.jp

ABSTRACT

Recent studies including our own report (I) have revealed that heavily phosphorus (P) doped Czochralski-silicon (HP-Cz-Si) exhibits peculiar defect behaviors during crystal growth. HP-Cz-Si crystals with a low resistivity of around $0.6 \text{ m}\Omega \text{ cm}$ (P concentration of $1.3 \times 10^{20} \text{ P cm}^{-3}$) have interstitial-type stacking faults (SFs) and dislocations, which degrade device characteristics. The purpose of this paper is to clarify what causes the defect behavior in HP-Cz-Si through theoretical calculations. The thermal equilibrium concentrations of substitutional P (P_s), interstitial P (P_i), and $(P_s)_n$ -vacancy (V) clusters ($n = 1-4$) were determined by using density functional theory (DFT) calculations. The concentrations of P_i ($[P_i]$) and $(P_s)_n V$ ($[(P_s)_n V]$) balanced with the given P_s concentration ($[P_s]$) were obtained as a function of the total P concentration ($[P]$) and the temperature. On the basis of the calculated results those can quantitatively explain our experimental results in the report (I), we propose a defect model that accurately represents HP-Cz-Si crystal growth. The main feature of the model is that the incorporated P_i atoms at the solid/liquid interface around $[P_i] = 10^{17} \text{ P}_i \text{ cm}^{-3}$ cause the formation of SFs and dislocations during the HP-Cz-Si crystal growth with around $[P] = 10^{20} \text{ P cm}^{-3}$. Furthermore, DFT calculations were performed for P_i segregation on the SF and for the photoelectron spectra of P 1s measured by hard x-ray photoelectron spectroscopy to explain the other experimental results in the report (I).

© 2024 Author(s). All article content, except where otherwise noted, is licensed under a Creative Commons Attribution (CC BY) license (<https://creativecommons.org/licenses/by/4.0/>). <https://doi.org/10.1063/5.0200130>

03 August 2024 06:46:51

I. INTRODUCTION

From the late 1970s to the early 2010s, many experimental studies have been conducted on the impact of dopants and impurities on intrinsic point defect behavior and grown-in defect formation during Si crystal growth.¹⁻⁸ The types of dopants that have been reported are p-type (B and Ga), neutral (C, Ge, and Sn), and n-type (P, As, Sb, and Bi). The impacts of impurities (H, C, O, and N) have also been investigated for the purpose of improving the quality of Si crystals.^{4,9-15} Among the p-type and n-type dopants, B, P, and As can be doped at the highest concentration. The highest concentration of B, P, and As for which experimental results have been reported up until the early 2010s was about

$1 \times 10^{19} \text{ B cm}^{-3}$, $3.5 \times 10^{19} \text{ P cm}^{-3}$ and $3 \times 10^{19} \text{ As cm}^{-3}$, respectively.⁴ Based on a model that quantitatively explains the intrinsic point defect behavior using density functional theory (DFT) calculations,¹⁶ the concentration distribution of intrinsic point defects valid for all pulling conditions in large-diameter Czochralski-Si (Cz-Si) crystal growth has been determined by computer simulation.^{17,18} Theoretical studies showed that the self-interstitial (I) and vacancy (V) formation energies around dopant atoms change depending on the type and size of the dopants, i.e., the electrical state and the local strain around the dopants. That is, the Si crystal becomes I -rich by B doping up to $1 \times 10^{19} \text{ B cm}^{-3}$ while it becomes V -rich by P doping up to $3.5 \times 10^{19} \text{ P cm}^{-3}$ and As doping up to $3 \times 10^{19} \text{ As cm}^{-3}$.

In the last decade, heavily P doped (HP-Cz-Si) crystals have been widely used in power devices. To reduce the power consumption, the crystal resistivity must be reduced as much as possible. Currently, the most advanced crystals can be manufactured with a resistivity as low as $0.6 \text{ m}\Omega \text{ cm}$ ($1.3 \times 10^{20} \text{ P cm}^{-3}$). The defect behavior in CZ-Si has been reported to change significantly when the P concentration in the Si crystal exceeds $3 \times 10^{19} \text{ P cm}^{-3}$.^{4,19–26} That is, the void formation is significantly suppressed with P doping over $(3\text{--}4) \times 10^{19} \text{ P cm}^{-3}$.^{4,19} Senda *et al.*²⁰ observed plate-like SiP²¹ precipitates of 100–200 nm in as-grown HP-CZ-Si crystals at around $8 \times 10^{19} \text{ P cm}^{-3}$. Zeng *et al.*^{22,23} also reported the formation of oxygen precipitates from heterogeneous nuclei of small SiP precipitates during the heat treatment of HP-Cz-Si crystals. Subsequently, Wu *et al.*²⁴ also reported that post-annealing of HP-CZ-Si crystals with a maximum [P] of $7.35 \times 10^{19} \text{ P cm}^{-3}$ at $450\text{--}1050^\circ\text{C}$ resulted in the formation of SiP precipitates of various crystallographic morphologies with dependent of temperature. Voronkov *et al.*²⁵ and Nakamura *et al.*²⁶ claimed that the increase of interstitial P (P_i) concentration causes the change of defect behavior from V-type to I-type in HP-Cz-Si.

Furthermore, in the $10^{20} \text{ P cm}^{-3}$ order, we have identified even more peculiar defect behavior in the report (I).²⁷ It was experimentally found that, at $1.3 \times 10^{20} \text{ P cm}^{-3}$, small dislocation loops were observed in the bottom, while interstitial-type stacking faults (SFs) with P segregation were observed in the middle of crystal. The growing and tangling dislocations and P segregation were also observed in the crystal portion for a longer thermal history around 600°C . The P segregation suggests the existence of supersaturated interstitial P_i atoms. However, no quantitative explanation of P_i concentration during HP-Cz-Si crystal growth has been given. Furthermore, various points still need to be clarified, such as the formation of SFs, the expansion of dislocations, and the actual state of defects in low-temperature regions during crystal growth of HP-Cz-Si.

In the present paper, the thermal equilibrium concentrations of substitutional P (P_s), interstitial P (P_i), and $(\text{P}_s)_nV$ ($n = 1\text{--}4$) clusters in Si are obtained on the basis of DFT calculations. We propose an appropriate model of intrinsic point defect behavior in growing HP-Cz-Si. Furthermore, we perform DFT calculations for P_i segregation on the SF and for the photoelectron spectra of P 1s measured by hard x-ray photoelectron spectroscopy (HAXPES) to explain the other experimental results in the report (I).²⁷

II. CALCULATION DETAILS

A. Formation energy and formation entropy of P_s , P_i , and $(\text{P}_s)_nV$ clusters

DFT calculations were carried out within the generalized gradient approximation (GGA)²⁸ for electron exchange and correlation using the CAMbridge Serial Total Energy Package (CASTEP) code.²⁹ Three-dimensional periodic boundary conditions were set with cubic supercells of 512 Si atoms to calculate the total energy of Si crystals containing P_s , P_i , and $(\text{P}_s)_nV$ clusters. The cut-off energy of the plane waves was 340 eV. We carried out k -point sampling at the Γ point. Note that if the

model contains one P atom, its concentration $[\text{P}] = 1 \times 10^{20} \text{ P cm}^{-3}$ is close to the actual concentration of the heavily P doped Si crystal. The formation energy of these P defects was obtained after geometry optimization.

Figure 1(a) shows the most stable isolated P_i atom which has the $\langle 110 \rangle$ dumbbell structure with a Si atom. The formation energies of the P_i atom [$E_f(\text{P}_i)$] and $(\text{P}_s)_nV$ clusters ($E_f((\text{P}_s)_nV)$) in Si were calculated with reference to the $E_f(\text{P}_s)$ of uniformly distributed P_s atoms in Si. E_f of the isolated P_i and P_i up to 5th nearest substituted P_s [Figs. 1(b)–1(f)] were obtained from

$$E_f(\text{P}_i) - E_f(\text{P}_s) = E_{\text{tot}}[\text{Si}_{512}\text{P}_i] - E_{\text{tot}}[\text{Si}_{511}\text{P}_s] - \frac{1}{512}E_{\text{tot}}[\text{Si}_{512}] \quad (1a)$$

and

$$E_f^{i\text{th}}(\text{P}_i) - E_f(\text{P}_s) = E_{\text{tot}}[\text{Si}_{511}\text{P}_i^{i\text{th}}\text{P}_s] - 2 \times E_{\text{tot}}[\text{Si}_{511}\text{P}_s] + \frac{511}{512}E_{\text{tot}}[\text{Si}_{512}] \quad (1b)$$

Here, $E_{\text{tot}}[\text{Si}_{512}]$, $E_{\text{tot}}[\text{Si}_{512}\text{P}_i]$, $E_{\text{tot}}[\text{Si}_{511}\text{P}_s]$, and $E_{\text{tot}}[\text{Si}_{511}\text{P}_i^{i\text{th}}\text{P}_s]$ correspond to the total energies of the perfect cell and cells including one P_i , one P_s , and one P_i at the i th nearest P_s , respectively. E_f of the $(\text{P}_s)_nV$ clusters up to $n=4$ [Figs. 2(a)–2(d)] were obtained from

$$\begin{aligned} E_f((\text{P}_s)_nV) - n \times E_f(\text{P}_s) &= E_{\text{tot}}[\text{Si}_{511-n}(\text{P}_s)_nV] \\ &\quad - n \times E_{\text{tot}}[\text{Si}_{511}\text{P}_s] \\ &\quad + \left(n \times E_{\text{tot}}[\text{Si}_{512}] - \frac{511}{512}E_{\text{tot}}[\text{Si}_{512}] \right). \end{aligned} \quad (1c)$$

Here, $E_{\text{tot}}[\text{Si}_{511-n}(\text{P}_s)_nV]$ corresponds to the total energy of the cell including one $(\text{P}_s)_nV$ cluster.

Due to the high calculation cost of the linear response method,³⁰ formation (vibration) entropies of P_s atom [$S_f(\text{P}_s)$] and P_i atom [$S_f(\text{P}_i)$] were calculated using a cubic supercell of 64 Si atoms. The change of formation entropy through $(\text{P}_s)_nV$ cluster formation was not taken into consideration due to its low calculation accuracy of relatively large $(\text{P}_s)_nV$ cluster sizes for a 64-Si atom model.

The thermal equilibrium concentrations of the P_s , P_i , and $(\text{P}_s)_nV$ clusters were obtained on the basis of the calculated E_f and S_f . The detail procedure will be described in Sec. III A.

B. Energy reduction in P_i cluster growth on SF

An interstitial-type Frank-loop stacking fault (SF) was modeled as shown in Fig. 3 and compared with the perfect Si model. The SF model and perfect model consist of 32 and 30 (111) layers, respectively, including 16 atoms in each layer. To obtain the energy reduction of P_i at the SF with reference to the Si bulk, formation energy [$E_f(\text{P}_i)$] of the P_i atom in Eq. (1a) was calculated by moving the position of the P_i atom from the bulk to the SF.

03 August 2024 06:46:51

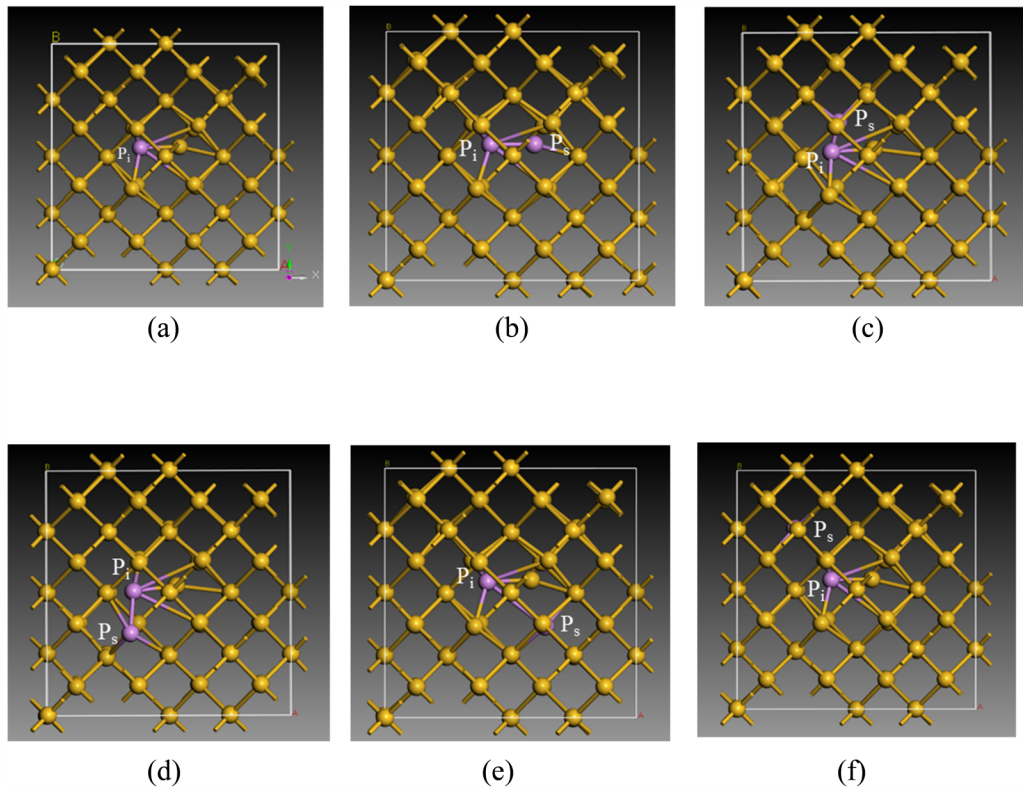


FIG. 1. Most stable P_i atoms shown by purple balls in 64-Si atom models. (a) Isolated P_i atom which has the (110) dumbbell structure with a Si atom and (b)–(f) P_i atom at 1st, 2nd, 3rd, 4th, and 5th nearest P_s atom.

03 August 2024 06:46:51

By adding the other P_i atoms to the P_i atom on the SF, the most stable $(P_i)_2$ – $(P_i)_7$ clusters on the SF were obtained among the cluster structures considered. The energy reduction in P_i cluster growth on the SF was then calculated.

C. Binding energy of P 1s electron for P_s , P_i , and $(P_s)_n V$ clusters

The binding energies of the P 1s electron (E_b) for P_s , P_i , and $(P_s)_n V$ clusters were calculated using the following formula:³¹

$$E_b = \Delta E_{\text{valence}} + \Delta E_{\text{core}}(P), \quad (2a)$$

where $\Delta E_{\text{valence}}$ is the valence energy difference between the excited state (the $N - 1$ electron system) and the ground state (the N electron system), and $\Delta E_{\text{core}}(P)$ is defined as follows:

$$\Delta E_{\text{core}}(P) = \Delta E_{\text{all orbitals}}(P) - \Delta E_{\text{valence}}(P), \quad (2b)$$

where $\Delta E_{\text{all orbitals}}(P)$ is the all-electron energy difference between the excited and the ground states for an isolated P atom and $\Delta E_{\text{valence}}(P)$ is the valence energy difference between the excited and the ground states for an isolated P atom.

III. RESULTS AND DISCUSSION

A. Concentrations of P_s , P_i , and $(P_s)_n V$ clusters and mechanism of peculiar defect behaviors during HP-Cz-Si crystal growth

Table I summarizes the calculated results of formation energy (E_f), formation entropy (S_f), site number (N), and degeneracy number (w_i) of the isolated P_s atom, isolated P_i atom, and P_i atoms around the P_s atom. E_f and w_i of $(P_s)_n V$ clusters are included. Here, we considered only neutral defects. Experimental³² and calculated³³ data from the literature are also included. The thermal equilibrium concentrations C_{P_s} of P_s , C_{P_i} of P_i , and $C_{(P_s)_n V}$ of $(P_s)_n V$ are calculated using the following formulas.^{16,33} Note that C_{P_i} depends on the given P_s concentration [P_s],

$$C_{P_s} = C_{\text{Si}} \exp\left(\frac{S_f(P_s)}{k}\right) \exp\left(-\frac{E_f(P_s)}{kT}\right), \quad (3a)$$

$$C_{P_i} = [P_s] \times \sum_{i=1}^{i=5} w_i \exp\left(\frac{S_f^{\text{ith}}(P_i)}{k}\right) \exp\left(-\frac{E_f^{\text{ith}}(P_i)}{kT}\right) + 12 \times (C_{\text{Si}} - 35 \times [P_s]) \times \exp\left(\frac{S_f(P_i)}{k}\right) \exp\left(-\frac{E_f(P_i)}{kT}\right), \quad (3b)$$

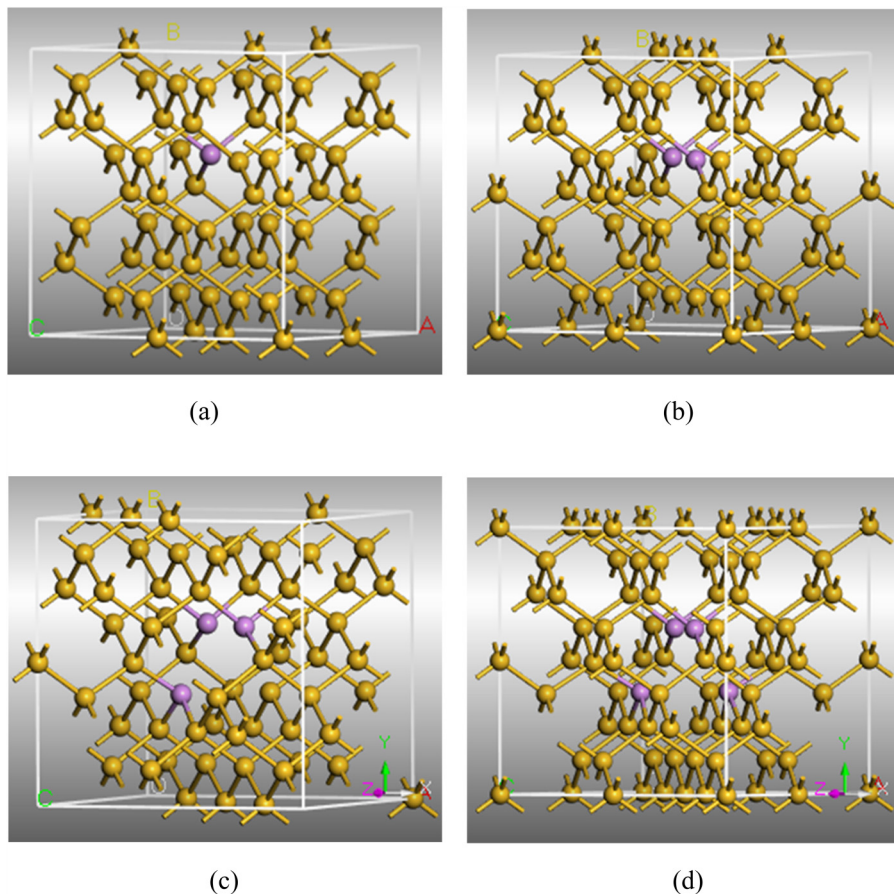


FIG. 2. Most stable $(P_s)_nV$ clusters (P_s atoms are shown by purple balls) in 64-Si atom models. (a) P_sV , (b) $(P_s)_2V$, (c) $(P_s)_3V$, and (d) $(P_s)_4V$.

03 August 2024 06:46:51

and

$$C_{(P_s)_nV} =_4 C_n \times C_{Si} \exp\left(\frac{S_f((P_s)_nV)}{k}\right) \exp\left(-\frac{E_f((P_s)_nV)}{kT}\right). \quad (3c)$$

Here, $C_{Si} = 5 \times 10^{22} \text{ cm}^{-3}$ is the site number of Si [= site number of P_s in Eq. (3a), site number of P_i in Eq. (3b), and site number of V in Eq. (3c)], k is the Boltzmann constant, and T is the temperature. The first row of Eq. (3b) indicates the C_{Pi} of P_i atoms up to the 5th nearest substituted P_s atom, and the second row of Eq. (3b) indicates the C_{Pi} of P_i atoms beyond the 5th nearest substituted P_s atom. Here, we assumed that E_f of the P_i farther than the 5th nearest is not affected by the P_s atom. $_4C_n$ in Eq. (3c) is the degeneracy number of n P_s atoms at the nearest V.

The experimental data of the thermal equilibrium concentration has been reported only for P_s as in Eq. (4a),³²

$$C_{Ps} = 1.8 \times 10^{22} \exp\left(-\frac{0.4 \text{ eV}}{kT}\right) \text{ cm}^{-3}. \quad (4a)$$

We used the value of $E_f = 0.4 \text{ eV}$ for the P_s atom in Eq. (4a) and the values of calculated changes of E_f and S_f summarized in

Table I to obtain the ratios C_{Pi}/C_{Ps} and $C_{(P_s)_nV}/(C_{Ps})^n$. C_{Pi}/C_{Ps} can be written by using Eqs. (3a) and (3b) as

$$\begin{aligned} \frac{C_{Pi}}{C_{Ps}} &= \frac{[P_s]}{C_{Si}} \times \sum_{i=1}^{i=5} w_i \exp\left(\frac{S_f^{ith}(P_i) - S_f(P_s)}{k}\right) \\ &\times \exp\left(-\frac{E_f^{ith}(P_i) - E_f(P_s)}{kT}\right) + 12 \times \left(1 - 35 \times \frac{[P_s]}{C_{Si}}\right) \\ &\times \exp\left(\frac{S_f(P_i) - S_f(P_s)}{k}\right) \exp\left(-\frac{E_f(P_i) - E_f(P_s)}{kT}\right). \end{aligned} \quad (4b)$$

Here, we assumed that S_f of P_i does not change [$S_f^{ith}(P_i) = S_f(P_i)$] even with the interaction with P_s . By the mass action law for the reaction of $P_s + I \rightleftharpoons P_i$, we obtained equilibrium P_i concentration $[P_i]$ balanced to the given $[P_s]$ as the following formula,

$$[P_i] = [P_s] \frac{C_{Pi}}{C_{Ps}}. \quad (4c)$$

Here, we assumed that the concentration of I maintained the thermal equilibrium concentration as the supersaturated I atoms

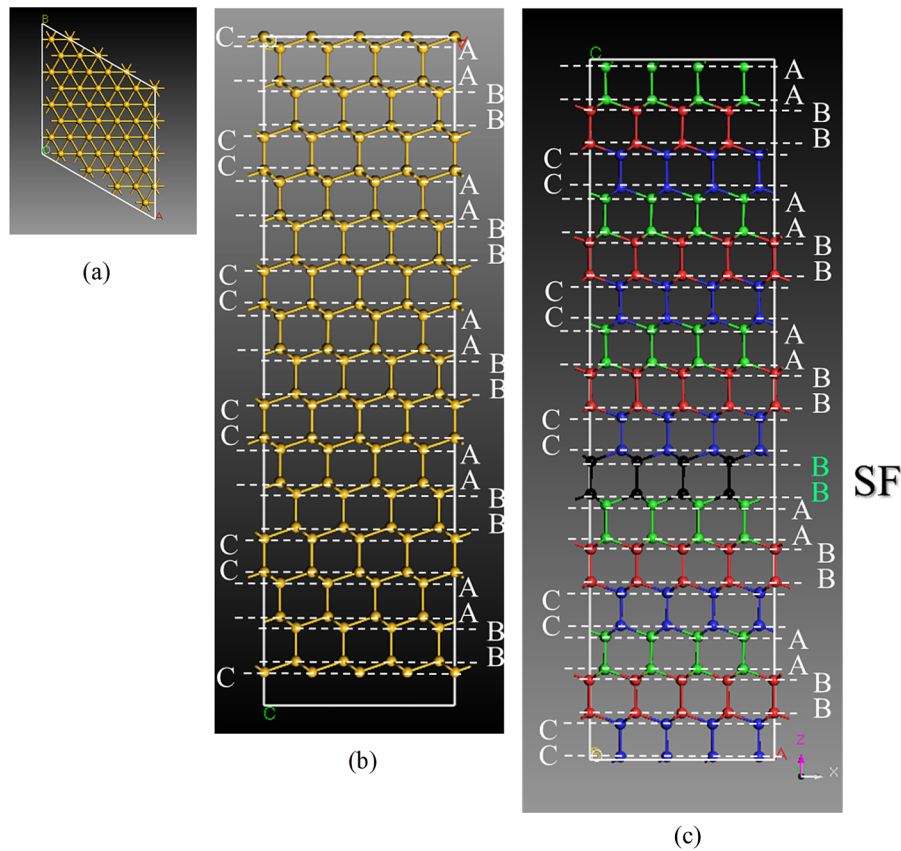


FIG. 3. Model of interstitial-type Frank-loop stacking fault (SF) compared with the perfect Si model. (a) The (111) plane including 16 atoms, (b) the perfect model consisting of 30 (111) layers, and (c) the SF model consisting of 32 (111) layers.

03 August 2024 06:46:51

TABLE I. Calculated results of formation energy E_f (eV), formation entropy S_f , site number (N), and degeneracy number (w_i) of P_s , P_i , and $(P_s)_n V$ clusters. Note that n in $E_f - nE_f(P_s)$ is the number of P_s atoms.

P defect	E_f	$E_f - nE_f(P_s)$	S_f/k	$S_f/k - S_f(P_s)/k$	N	w_i
Isolated P_s	0.4 (Exp. ³²)		1.48	-1.02 (Exp. ³²)		
Isolated P_i	2.99 ^a	2.59	5.95	4.47	1	12
P_i at 1st of P_s	1.48 ^a	1.08			1	6
P_i at 2nd of P_s	1.81 ^a	1.41			4	48
P_i at 3rd of P_s	2.29 ^a	1.89			12	144
P_i at 4th of P_s	2.32 ^a	1.92			12	144
P_i at 5th of P_s	2.46 ^a	2.06			6	7
$P_s V$	2.86 ^a	2.46				4
		2.31 (Cal. ³³)				
$(P_s)_2 V$	1.85 ^a	1.05				6
		0.97 (Cal. ³³)				
$(P_s)_3 V$	1.47 ^a	0.27				4
		-0.18 (Cal. ³³)				
$(P_s)_4 V$	0.39 ^a	-1.21				1
		-1.68 (Cal. ³³)				

^aThe data of E_f were obtained by using experimental data of $E_f = 0.4$ eV for P_s .

were absorbed by the SFs and/or dislocation loops as will be mentioned later in this section.

The ratio $C_{(P_s)_n}V/(C_{P_s})^n$ can be written by using Eqs. (3a) and (3c) as

$$\frac{C_{(P_s)_n}V}{(C_{P_s})^n} = C_n \times C_{Si} \left(\frac{1}{C_{Si}} \right)^n \times \exp \left(\frac{S_f((P_s)_n V) - n \times S_f(P_s)}{k} \right) \times \exp \left(- \frac{E_f((P_s)_n V) - n \times E_f(P_s)}{kT} \right). \quad (4d)$$

Here, we neglected the change in formation entropy caused by $(P_s)_n V$ formation for the reason described in Sec. II A. By the mass action law for the reaction of $n P_s \rightleftharpoons (P_s)_n V + I$,^{33,34} we obtained the equilibrium $(P_s)_n V$ concentration $[(P_s)_n V]$ balanced to the given $[P_s]$ as the following formula:

$$[(P_s)_n V] = [P_s]^n \times \frac{C_{(P_s)_n}V}{(C_{P_s})^n} = C_n \times C_{Si} \left(\frac{[P_s]}{C_{Si}} \right)^n \times \exp \left(- \frac{E_f((P_s)_n V) - n \times E_f(P_s)}{kT} \right). \quad (4e)$$

Here, we also assumed that the concentration of I maintained the thermal equilibrium concentration.

The total P concentration $[P]^{\text{tot}}$ can be obtained by

$$[P]^{\text{tot}} = [P_s] + [P_i] + n \sum_{n=1}^{n=4} [(P_s)_n V]. \quad (5)$$

The thermal equilibrium concentration C_{P_i} of P_i was calculated using Eq. (3b). Figure 4 shows C_{P_i} as a function of $1/T$ for $[P_s] = 1 \times 10^{19}, 5 \times 10^{19}, 1 \times 10^{20}$, and $2 \times 10^{20} \text{ P}_s \text{ cm}^{-3}$. The dotted lines indicate the best fitted C_{P_i} with an exponential function

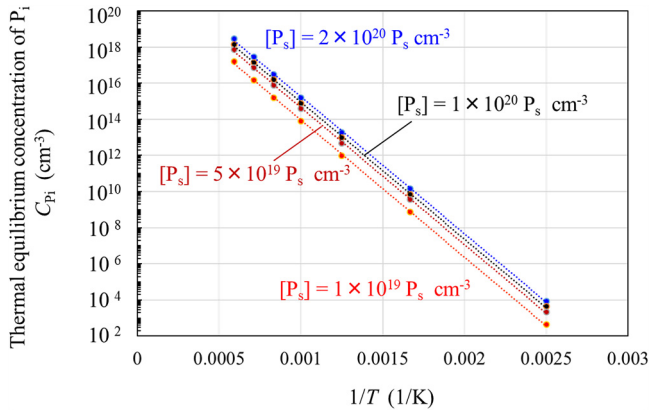


FIG. 4. Thermal equilibrium concentrations C_{P_i} of P_i as a function of $1/T$. The dotted lines indicate the best fitted lines of calculated C_{P_i} with exponential function approximation.

approximation. The C_{P_i} can be summarized in one expression as

$$C_{P_i} = 3.56 \times 10^2 [P_s] \exp \left(- \frac{1.51 \text{ eV}}{kT} \right) \text{ cm}^{-3}, \quad (6)$$

between 1×10^{19} and $2 \times 10^{20} \text{ P}_s \text{ cm}^{-3}$.

The thermal equilibrium concentrations $C_{(P_s)_n}V$ of $(P_s)_n V$ were obtained by using Eq. (3c) and neglecting the formation entropy change,

$$C_{P_s}V = 2 \times 10^{23} \exp \left(- \frac{2.86 \text{ eV}}{kT} \right) \text{ cm}^{-3}, \quad (7a)$$

$$C_{(P_s)_2}V = 3 \times 10^{23} \exp \left(- \frac{1.85 \text{ eV}}{kT} \right) \text{ cm}^{-3}, \quad (7b)$$

$$C_{(P_s)_3}V = 2 \times 10^{23} \exp \left(- \frac{1.47 \text{ eV}}{kT} \right) \text{ cm}^{-3}, \quad (7c)$$

and

$$C_{(P_s)_4}V = 5 \times 10^{22} \exp \left(- \frac{0.39 \text{ eV}}{kT} \right) \text{ cm}^{-3}. \quad (7d)$$

Figure 5 shows the thermal equilibrium concentrations, C_p of P_s [Eq. (4a)], C_{P_i} of P_i [Eq. (6)], and $C_{(P_s)_n}V$ of $(P_s)_n V$ [Eqs. (7a)–(7d)] as a function of temperature. For C_{P_i} , the values of $[P_s]$ at $1 \times 10^{19}, 5 \times 10^{19}, 1 \times 10^{20}$, and $2 \times 10^{20} \text{ P}_s \text{ cm}^{-3}$ are shown. Here, we assumed that the melting temperature T of HP-Cz-Si is 1412 °C. By using the thermal equilibrium concentration at the melting temperature, we obtained the incorporated P defect concentrations, $[P_s]$ of P_s , $[P_i]$ of P_i , and $[(P_s)_n V]$ of $(P_s)_n V$ as functions of total P concentrations $[P]^{\text{tot}}$ as shown in Fig. 6(a). Here, we calculated $[P_i]$ by Eq. (4c), $[(P_s)_n V]$ by Eq. (4e), and $[P]^{\text{tot}}$ by Eq. (5) at the given $[P_s]$. We clarified that the main P defects incorporated at the solid/liquid interface are P_s and P_i in the $[P]^{\text{tot}}$ range of 1×10^{19} – $2 \times 10^{20} \text{ P cm}^{-3}$. Figure 6(b) shows the P defect concentrations, $[P_s]$ of P_s , $[P_i]$ of P_i , and $[(P_s)_n V]$ of $(P_s)_n V$ as functions of total P concentrations $[P]^{\text{tot}}$ at $T = 600$ °C. Figure 6(c) shows P_s , P_i , and $(P_s)_4 V$ concentrations at $[P]^{\text{tot}} = 1 \times 10^{20} \text{ P cm}^{-3}$ as a function of temperature. The obtained expressions, C_p [Eq. (4a)], C_{P_i} [Eq. (6)], and $C_{(P_s)_n}V$ [Eqs. (7a)–(7d)], will be very impactful to expand the application of numerical simulation¹⁸ to HP-Cz-Si crystal growth. Here, we use these data in the following discussion on the mechanism of defect behaviors in HP-Cz-Si crystal growth.

Table II summarizes the incorporated P_s and P_i concentration at the melting temperature with their supersaturated temperatures. The data in Table II can be used quantitatively to explain our experimental results in the report (I)²⁷ of the peculiar defect behavior around $10^{20} \text{ P cm}^{-3}$ mentioned in Sec. I.

At the melting temperature, P_i around 10^{17} cm^{-3} is incorporated at the solid/liquid interface by heavily P doping around $10^{20} \text{ P cm}^{-3}$. V becomes supersaturated at a concentration of about 10^{14} – $10^{15} \text{ V cm}^{-3}$ after the pair recombination with I .^{4,35} P_i atoms become supersaturated at a concentration of about $10^{17} \text{ P}_i \text{ cm}^{-3}$

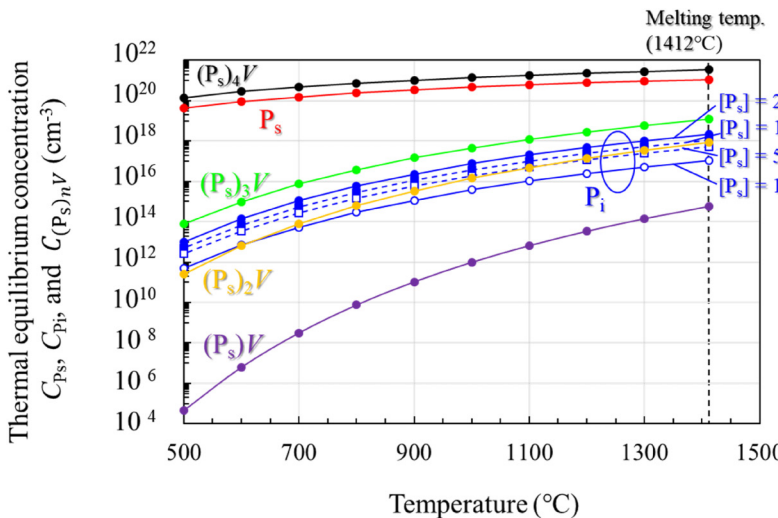


FIG. 5. Thermal equilibrium concentrations of P_s , P_i , and $(P_s)_nV$ as a function of temperature.

around void formation temperatures (around 1100 °C).³⁶ Since the calculated diffusion barrier of P_i atom is very small (0.14 eV), the reaction $P_i + V \rightarrow P_s$ proceeds, and the observable voids no longer form during crystal growth. Note that P_i still remains at $[P_i] \sim 10^{17} \text{ P}_i \text{ cm}^{-3}$ after the reaction $P_i + V \rightarrow P_s$.

During cooling of the crystal down to about 600 °C, the supersaturated P_i kicks out a lattice Si atom ($P_i \rightarrow P_s + I$). The $[P_i]$ is decreasing as can be seen from Fig. 6(c). The I becomes supersaturated and forms I -type dislocation loops and SFs.²⁷ The concentration of I maintained the thermal equilibrium concentration as the supersaturated I atoms were absorbed by the SFs and/or dislocation loops.

At temperatures of 600 °C and lower, P_s becomes supersaturated. As can be seen from Figs. 6(b) and 6(c), the $(P_s)_4V$ concentration balanced to that of P_s is about $10^{19} \text{ P}_4V \text{ cm}^{-3}$ when $[P]^{\text{tot}} = 10^{20} \text{ P cm}^{-3}$. That is, a $(P_s)_4V$ cluster forms from the reaction $4P_s \rightarrow (P_s)_4V + I$ at 600 °C and lower. We will further discuss of the formation of $(P_s)_4V$ in Sec. III C. The generated I is absorbed by the I -type dislocation loops, causing defect growth and tangle. In addition, the P_i formed by $P_s + I \rightarrow P_i$ segregates on SFs.²⁷ The clustering of P_i atoms on SF will be discussed in Sec. III B. The formation of $(P_s)_4V$ drastically proceeds during long-time wafer annealing at 600 °C and lower.²⁷

Finally, we briefly discuss the case when $[P]^{\text{tot}}$ is less than $5 \times 10^{19} \text{ P cm}^{-3}$. As shown in Table II, P_i becomes supersaturated when below the void formation temperatures (around 1100 °C). Therefore, supersaturated V forms voids and later the reaction $P_i \rightarrow P_s + I$ occurs during crystal growth. This is probably the reason that voids were experimentally observed at $[P]^{\text{tot}}$ less than $5 \times 10^{19} \text{ P cm}^{-3}$.⁴

B. P_i segregation on SF

Figure 7 shows the most stable configuration of the P_i atom at the SF and the formation energy of the P_i atom with reference that on the SF. We found that the P_i atom becomes about 0.3 eV more stable when the P_i atom is trapped on the SF. The energy is not

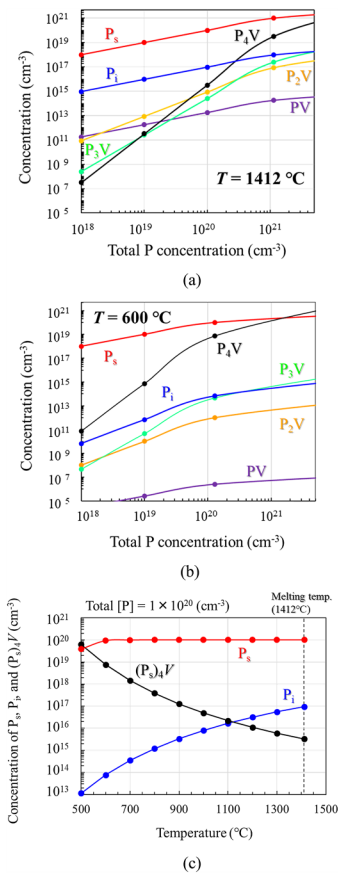


FIG. 6. Incorporated P defect concentrations at the solid/liquid interface at melting temperature ($T = 1412^\circ\text{C}$) (a), P defect concentrations at $T = 600^\circ\text{C}$, as functions of total P concentrations (b), and P_s , P_i , $(P_s)_4V$ concentrations at a total $[P] = 1 \times 10^{20} \text{ cm}^{-3}$ as a function of temperature (c).

TABLE II. Incorporated P_s and P_i concentration at melting temperature ($T = 1412^\circ\text{C}$) with total P concentration of $[P]^\text{tot} = 2.0 \times 10^{20}$, 1.0×10^{20} , 5.0×10^{19} , and 1.0×10^{19} P cm^{-3} . Supersaturated temperatures of P_s and P_i are also included.

$[P]^\text{tot}$ (cm^{-3})	Incorporated $[P_s]$ (cm^{-3})	Supersaturated temp. of P_s ($^\circ\text{C}$)	Incorporated $[P_i]$ (cm^{-3})	Supersaturated temp. of P_i ($^\circ\text{C}$)
2.0×10^{20}	$\approx 2.0 \times 10^{20}$	758	3.8×10^{18}	1169
1.0×10^{20}	$\approx 1.0 \times 10^{20}$	620	9.5×10^{16}	1091
5.0×10^{19}	$\approx 5.0 \times 10^{19}$	515	2.4×10^{16}	1021
1.0×10^{19}	$\approx 1.0 \times 10^{19}$	346	9.5×10^{14}	884

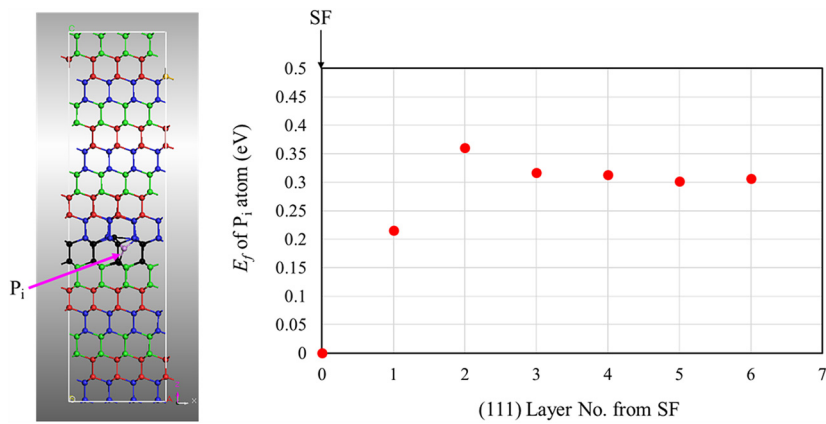


FIG. 7. Most stable configuration of P_i atom at the SF (left), and the formation energy of P_i atom based on that on SF (right).

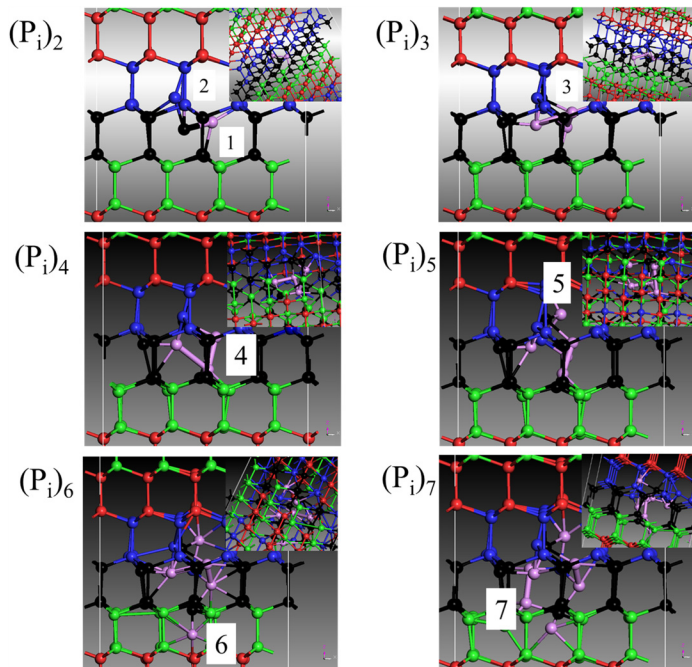


FIG. 8. Obtained stable structures of $(P_i)_2$ to $(P_i)_7$ clusters on SF.

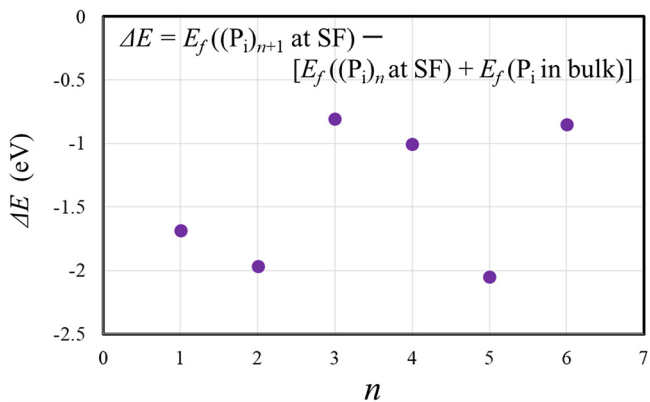


FIG. 9. Energy reduction $\Delta E = E_f((P_i)_{n+1} \text{ at SF}) - [E_f((P_i)_n \text{ at SF}) + E_f(P_i \text{ in bulk})]$ per P_i atom in P_i cluster growth up to $(P_i)_7$ on SF.

greatly reduced but it will be a sufficient driving force for trapping as the supersaturation of P_i increases as the temperature decreases during crystal growth.

By adding the other P_i atoms one by one to the P_i atom on the SF, we discovered stable $(P_i)_2-(P_i)_7$ clusters on the SF as shown in Fig. 8. Figure 9 shows the energy reduction

$$\Delta E = E_f((P_i)_{n+1} \text{ at SF}) - [E_f((P_i)_n \text{ at SF}) + E_f(P_i \text{ in bulk})] \quad (8)$$

per P_i atom in the P_i cluster growth on the SF. We found that the energy is reduced by about 0.8–2.0 eV per P_i atom associated with the P_i cluster growth. This result indicates that if one P_i is trapped on the SF, the P_i cluster growth will be drastic.

C. Photoelectron spectra of P 1s measured by HAXPES

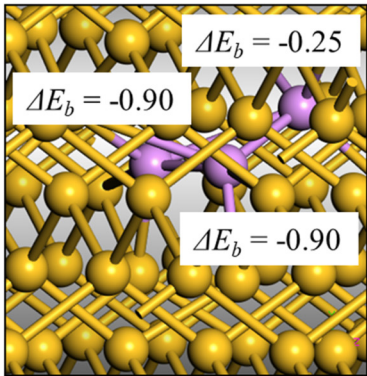
Table III summarizes the calculated binding energies of the P 1s electron (E_b) for P_s , P_i , and $(P_s)_n V$ clusters, and energy shift ΔE_b from the value of P_s . $(P_s + P_i) + P_s(a)$ and $(P_s + P_i) + P_s(b)$ ²⁷ indicate two types of P_3 clusters. Experimental data of P2 (inactive) include P2 (active) component as P2 (active) component could not be separated in P2 (inactive).²⁷

TABLE III. Calculated binding energies of P 1s electron (E_b) for P_s , P_i , and $(P_s)_n V$ clusters, and energy shift ΔE_b from the value of P_s . $(P_s + P_i) + P_s(a)$ and $(P_s + P_i) + P_s(b)$ ²⁷ indicate two types of P_3 clusters. Experimental data of P2 (inactive) include P2 (active) component as P2 (active) component could not be separated in P2 (inactive).²⁷

P defect	Charge	E_b (eV)	ΔE_b from E_b of P_s (eV)
P_s	+1	2152.61	
P1 (Exp. ²⁷)	+1	2144.6	
P_i	-1	2150.99	-1.62
$P_s V$	-1	2151.66	-0.95
$(P_s)_2 V$	0	2151.67	-0.94
$(P_s)_3 V$	-1	2151.67	-0.94
$(P_s)_4 V$	0	2151.64	-0.97
P2 (inactive) (Exp. ²⁷)	0	2143.4	-1.2
$(P_s + P_i) + P_s(a)$	+1	2151.71, 2151.71, 2152.36	-0.90, -0.90, -0.25
$(P_s + P_i) + P_s(b)$	+1	2151.65, 2151.78, 2152.57	-0.96, -0.83, -0.04
P2 (active) (Exp. ²⁷)	+1	2143.6	-1.0

03 August 2024 06:46:51

$(P_s + P_i) + P_s(a)$



$(P_s + P_i) + P_s(b)$

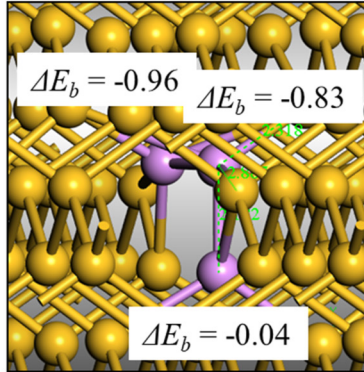


FIG. 10. Two types of P_3 clusters responsible for origin of P2 (active).

from the value of P_s . The charge state determined by the energy band calculations is also shown. By comparing the calculated results with the experimental HAXPES results [P1, P2 (inactive) and P2 (active) peaks] in the report (I),²⁷ we concluded that the origin of the P1 peak should be P_s . The origin of the P2 peak (inactive), which becomes noticeable after a longer thermal history at 600 °C and lower and/or long-time wafer annealing at 600 °C and lower, should be $(P_s)_4V$. $(P_s)_2V$ is not the origin of the P2 peak (inactive) as its concentration is very low as shown in Fig. 6(b).

The P2 peak (active) was also observed in the as-grown crystal.²⁷ Figure 10 shows two types of P_3 clusters, $(P_s + P_i) + P_s(a)$ and $(P_s + P_i) + P_s(b)$, which are responsible for the P2 peak (active). These two clusters are stable as the energy of $(P_s + P_i) + P_s(a)$ is reduced by -0.94 eV and that of $(P_s + P_i) + P_s(b)$ is reduced by -1.10 eV from the isolated one P_s and two P_i . Furthermore, they have a +1 charge and ΔE_b close to that of the experimental results. That is, the two clusters are possible origins of P2 (active) formed during crystal growth.

IV. CONCLUSION

HP-Cz-Si crystals with a resistivity down to $0.6\text{ m}\Omega\text{ cm}$ ($[P] = 1.3 \times 10^{20}\text{ P cm}^{-3}$) are currently being manufactured for application for low-voltage power MOSFETs. Recent studies including our own report (I)²⁷ have revealed that HP-Cz-Si exhibits peculiar defect behaviors such as the formation of SFs and dislocations. The purpose of this paper is to clarify the causes of the defect behavior in HP-Cz-Si through theoretical calculations.

The thermal equilibrium concentrations of P_s , P_i , and $(P_s)_nV$ ($n = 1-4$) clusters were determined by DFT calculations. Furthermore, equilibrium concentrations of P_i and $(P_s)_nV$ balanced to the given P_s concentration were obtained as functions of the total P concentration and the temperature. On the basis of the calculated results those can quantitatively explain our experimental results in the report (I),²⁷ we proposed the following defect model to represent HP-Cz-Si crystal growth. At the melting temperature, P_i around 10^{17} cm^{-3} is incorporated at the solid/liquid interface by heavily P doping around 10^{20} P cm^{-3} . From 1100 to 600 °C, supersaturated P_i atom interacts with the Si atom to become P_s with the emission of I . The emitted I_s agglomerate and form SFs and dislocations. At temperatures of 600 °C and lower, supersaturated P_s becomes $(P_s)_4V$ with the emission of I . The SFs and dislocations absorb I_s and become more complex defects. The supersaturated P_i also segregates on the defects. The formation of $(P_s)_4V$ further proceeds during long-time wafer annealing at 600 °C and lower.

The other DFT calculations explained the P_i segregation on the SF. The calculated energy is reduced by about 0.8–2.0 eV for each P_i associated with the growth of a P_i cluster up to $(P_i)_7$. That is, if one P_i is trapped on the SF, the growth of the P_i cluster will proceed drastically.

Finally, the binding energies of the P 1s electron for P_s , P_i , and $(P_s)_nV$ clusters were calculated and compared to the experimental HAXPES results [P1, P2 (inactive) and P2 (active) peaks] in the report (I).²⁷ We concluded that the origin of the P1 peak should be P_s , and the origin of the P2 peak (inactive), which becomes noticeable after longer thermal history at 600 °C and lower and/or long-time wafer annealing at 600 °C and lower,

should be $(P_s)_4V$. Lastly, we proposed two structures of the P_3 cluster responsible for the P2 peak (active) observed in the as-grown crystal.

ACKNOWLEDGMENTS

This work was partially supported by JST, CREST, Japan (Grant No. JPMJCR21C2).

AUTHOR DECLARATIONS

Conflict of Interest

The authors have no conflicts to disclose.

Author Contributions

Koji Sueoka: Conceptualization (lead); Data curation (lead); Formal analysis (lead); Funding acquisition (lead); Investigation (lead); Methodology (lead); Supervision (lead); Validation (lead); Writing – original draft (lead); Writing – review & editing (lead).

Yasuhiro Narushima: Investigation (supporting); Methodology (supporting); Validation (supporting). **Kazuhisato Torigoe:** Conceptualization (equal); Formal analysis (equal); Investigation (equal); Methodology (equal); Validation (equal).

Naoya Nonaka: Investigation (supporting); Methodology (supporting); Validation (supporting). **Koutaro Koga:** Investigation (supporting); Methodology (supporting); Validation (supporting). **Toshiaki Ono:** Conceptualization (equal); Formal analysis (equal); Investigation (equal); Methodology (equal); Validation (equal).

Hiroshi Horie: Formal analysis (equal); Investigation (supporting); Methodology (supporting); Validation (supporting). **Masataka Hourai:** Conceptualization (equal); Data curation (equal); Formal analysis (equal); Investigation (equal); Validation (equal); Writing – review & editing (equal).

03 August 2024 06:46:51

DATA AVAILABILITY

The data that support the findings of this study are available within the article.

REFERENCES

- 1 A. J. R. de Kock, W. T. Stacy, and W. M. van de Wijgert, *Appl. Phys. Lett.* **34**, 611 (1979).
- 2 T. Abe, H. Harada, and J. Chikawa, *Mater. Res. Soc. Proc.* **14**, 1 (1983).
- 3 E. Dornberger, D. Gräf, M. Suhren, U. Lambert, P. Wagner, F. Dupret, and W. von Ammon, *J. Cryst. Growth* **180**, 343 (1997).
- 4 K. Nakamura, R. Suetaka, T. Saishoji, and J. Tomioka, in *Proceedings of the Forum on the Science and Technology of Silicon Materials 2003* (Japan Technical Information Service, 2003), p. 161 and references therein.
- 5 W. Sugimura, T. Ono, S. Umeno, M. Hourai, and K. Sueoka, *ECS Trans.* **2**, 95 (2006).
- 6 L. Válek, D. Lysáček, and J. Šík, *J. Electrochem. Soc.* **154**, H904 (2007).
- 7 J. Vanhellemont, X. Zhang, W. Xu, J. Chen, X. Ma, and D. Yang, *J. Appl. Phys.* **108**, 123501 (2010).
- 8 T. Abe, *J. Cryst. Growth* **334**, 4 (2011).
- 9 M. Iida, W. Kusaki, M. Tamatsuka, E. Iino, M. Kimura, and S. Muraoka, *ECS Proc. PV99-1*, 499 (1999).
- 10 K. Nakai, Y. Inoue, H. Yokota, A. Ikari, J. Takahashi, A. Tachikawa, K. Kitahara, Y. Ohta, and W. Ohashi, *J. Appl. Phys.* **89**, 4301 (2001).
- 11 J. Takahashi, K. Kawakami, and K. Nakai, *J. Appl. Phys.* **89**, 5949 (2001).

- ¹²S. Umeno, T. Ono, T. Tanaka, E. Asayama, H. Nishikawa, M. Hourai, H. Katahama, and M. Sano, *J. Cryst. Growth* **236**, 46 (2002).
- ¹³V. V. Voronkov and R. Falster, *J. Cryst. Growth* **273**, 412 (2005).
- ¹⁴G. Kissinger, G. Raming, R. Wahlich, and T. Müller, *Mater. Sci. Forum* **725**, 221 (2012).
- ¹⁵W. Sugimura, T. Ono, K. Nakamura, M. Hourai, and K. Higashida, in *Proceedings of the Forum on the Science and Technology of Silicon Materials 2014* (Shukou-sha Corporation, 2014), p. 248.
- ¹⁶K. Sueoka, E. Kamiyama, and J. Vanhellemont, *J. Appl. Phys.* **114**, 153510 (2013) and references therein.
- ¹⁷K. Sueoka, Y. Mukaiyama, S. Maeda, M. Iizuka, and V. M. Mamedov, *ECS J. Solid State Sci. Technol.* **8**, P228 (2019).
- ¹⁸Y. Mukaiyama, K. Sueoka, S. Maeda, M. Iizuka, and V. M. Mamedov, *J. Cryst. Growth* **531**, 125334 (2020).
- ¹⁹M. Porrini, J. Duchini, and A. Bazzali, *Cryst. Res. Technol.* **49**, 564 (2014).
- ²⁰T. Senda, T. Ishikawa, H. Fujimori, H. Matsumura, S. Narimatsu, Y. Abe, and T. Horikawa, "Extended abstracts," in *The 78th JSAP Autumn Meeting* (The Japan Society of Applied Physics, 2017), 7p-PB6-5 (in Japanese).
- ²¹S. Liang and R. Schmid-Fetzer, *J. Phase Equilib. Diffus.* **35**, 24 (2014).
- ²²Y. Zeng, X. Ma, D. Tian, W. Wang, L. Gong, D. Yang, and D. Que, *J. Appl. Phys.* **105**, 093503 (2009).
- ²³Y. Zeng, X. Ma, J. Chen, W. Song, W. Wang, L. Gong, D. Tian, and D. Yang, *J. Appl. Phys.* **111**, 033520 (2012).
- ²⁴D. Wu, T. Zhao, B. Ye, H. Chen, X. Liang, S. Li, D. Tia, D. Yang, and X. Ma, *J. Appl. Phys.* **134**, 155701 (2023).
- ²⁵V. V. Voronkov, R. Falster, M. Porrini, and J. Duchini, *Phys. Status Solidi A* **209**, 1898 (2012).
- ²⁶K. Nakamura, S. Narimatsu, T. Senda, and S. Maeda, "Extended abstracts," in *The 80th JSAP autumn meeting* (The Japan Society of Applied Physics, 2019), 18a-C212-5 (in Japanese).
- ²⁷M. Hourai, Y. Narushima, K. Torigoe, N. Nonaka, K. Koga, T. Ono, H. Horie, and K. Sueoka, *J. Appl. Phys.* (in press) (2024).
- ²⁸J. Perdew, K. Burke, and M. Ernzerhof, *Phys. Rev. Lett.* **77**, 3865 (1996).
- ²⁹The CASTEP code is available from Dassault Systems Biovia Inc.
- ³⁰S. Baroni, S. de Gironcoli, A. dal Corso, and P. Giannozzi, *Rev. Mod. Phys.* **73**, 515 (2001).
- ³¹T. Mizoguchi, I. Tanaka, S.-P. Gao, and C. J. Pickard, *J. Phys.: Condens. Matter* **21**, 104204 (2009).
- ³²D. Nobili, *Crystal Growth and Characterization of Advanced Materials* (World Scientific Publishing Co. Pte. Ltd., 1988), p. 629.
- ³³R. Chen, B. Trzynadlowski, and S. T. Dunham, *J. Appl. Phys.* **115**, 054906 (2013).
- ³⁴Y. Takamura, S. H. Jain, P. B. Griffin, and J. D. Plummer, *J. Appl. Phys.* **92**, 230 (2002).
- ³⁵V. V. Voronkov, *J. Cryst. Growth* **59**, 625 (1982).
- ³⁶M. Hourai, T. Nagashima, E. Kajita, S. Miki, T. Shigematsu, and M. Okui, *J. Electrochem. Soc.* **142**, 3193 (1995).